Convergent Evolution Between Insect and Mammalian Audition

Fernando Montealegre-Z.,[1]*† Thorin Jonsson,[1] Kate A. Robson-Brown,[2] Matthew Postles,[1] Daniel Robert[1]*

In mammals, hearing is dependent on three canonical processing stages: (i) an eardrum collecting sound, (ii) a middle ear impedance converter, and (iii) a cochlear frequency analyzer. Here, we show that some insects, such as rainforest katydids, possess equivalent biophysical mechanisms for auditory processing. Although katydid ears are among the smallest in all organisms, these ears perform the crucial stage of air-to-liquid impedance conversion and signal amplification, with the use of a distinct tympanal lever system. Further along the chain of hearing, spectral sound analysis is achieved through dispersive wave propagation across a fluid substrate, as in the mammalian cochlea. Thus, two phylogenetically remote organisms, katydids and mammals, have evolved a series of convergent solutions to common biophysical problems, despite their reliance on very different morphological substrates.

Many animals have evolved auditory organs with highly sensitive micro- and nanoscopic mechanisms that are able to detect vanishingly weak acoustic energy (*1*) and perform frequency analysis (*2*). In mammals, the chain of auditory biophysical events starts with the transformation of airborne acoustic energy into the mechanical vibrations of an eardrum. The lever action of delicate middle ear bones passes these eardrum vibrations to the oval window (Fig. 1), generating force gain via surface area ratio. This is the critically important step of impedance conversion that enables the efficient transfer of acoustic energy from airborne vibrations to the liquid-immersed mechanosensory hair cells in the cochlea (*2*). A second salient feature of many auditory systems is their capacity to analyze the frequency content of incoming sound waves. This process makes use of the mechanical anisotropy of the fluid-bathed basilar membrane to spatially decompose the acoustic signal into its frequency components, a biological form of the Fourier transform (*3*). Cochlear hair cells receive mechanical inputs at specific frequencies, depending on their position along the stiffness gradient of the basilar membrane (*4*, *5*). This "piano keyboard" mapping, or tonotopic organization, is the canonical mechanism for frequency selectivity in mammals (*5*).

Impedance conversion is crucial to hearing in terrestrial mammals, yet it is unknown in insects. Here, we identify and characterize auditory mechanisms in an insect that are markedly convergent with those of mammalian ears. We studied the South American rainforest katydid *Copiphora gorgonensis* (Orthoptera: Tettigoniidae: Copiphorini) and show that impedance transformation arises from unconventional tympanal mechanics, relying on a lever and fulcrum system and a favorable surface-area ratio to amplify and drive vibrations into the auditory sensory organ (Fig. 1). Next, we show that frequency analysis is enabled by the action of a newly identified organ, a fluid-filled vesicle, joining with the mechanosensory organ to support dispersive wave propagation and tonotopy. Our results reveal a notable case of convergence, whereby organisms with the most remote phylogenetic histories (such as mammals and katydids), have evolved to hear in a markedly analogous way.

As in all katydids, the ears of *C. gorgonensis* are located on the prothoracic tibia; the male calling song is a 23-kHz tone, with some frequency modulation (FM) (Fig. 2A) (*6*). Spanning only 600 μm, these ears are among the smallest known in all animals (*7*). X-ray microcomputer tomography (μCT; 2.8-μm voxel resolution) of fresh specimens reveals external and internal auditory anatomy. Each ear presents a pair of tympanal membranes (TMs) backed by an air-filled tracheal pipe connecting through the leg to the first spiracle on each side of the body (Fig. 2C and fig. S1) (*8*, *9*). The mechanosensory organ, the crista acustica (CA), lies on the dorsal wall of the anterior tracheal branch (*10*, *11*) and contains 28 mechanoreceptor units (Fig. 2D and fig. S1). In contrast to other auditory insects, such as locusts, flies, and moths (*7*, *12*), katydid mechanoreceptors are not in direct contact with the TMs. In previous studies, the general morphological organization of the CA was found to be reminiscent of an uncoiled tapering basilar membrane (Fig. 2C) (*10*, *11*, *13*).

Here, we identify an organ in the katydid's ear: the acoustic vesicle (AV). The AV is derived from the hemolymphatic system, yet it is distinctly different. The AV is elongated and tapering, just like an uncoiled mammalian cochlea (Fig. 2, C and E). Preliminary apolar extraction (*14*) reveals that the AV contains a lipidic fluid, which is incompressible and would be suitable for high-velocity sound propagation. We have also shown that the AV is a functionally important organ in other katydid species (movie S1). The AV is located underneath the dorsal exocuticle of the tibia, adjacent to CA and between both TMs (Fig. 2, C and D), and connects with the hemolymph channel by a narrow constriction (Fig. 2, C to E). Notably, the AV is absent from both meso- and metathoracic legs, where no ears are found (fig. S2). Previous studies did not distinguish the AV from the conventional hemolymphatic supply (*10*, *13*).

We used laser Doppler vibrometry (LDV) to examine the vibrational behavior of the proximal tibia (Fig. 2E) and to establish the functional importance of morphological components linking the TM to the CA (*14*). First, we measured tympanal mechanics in response to controlled

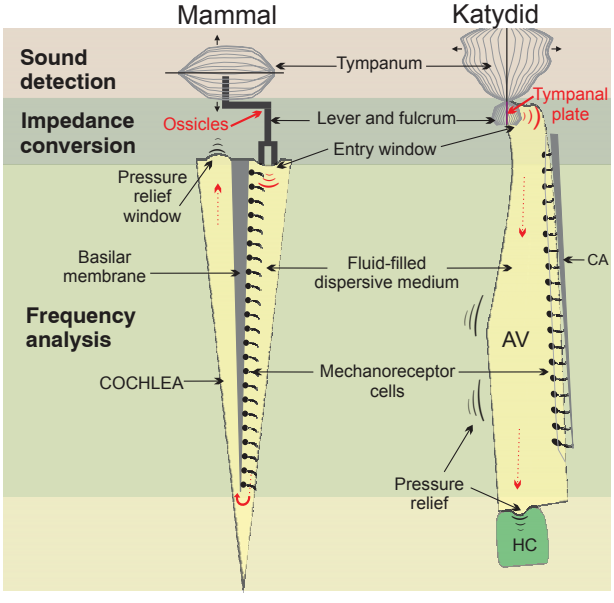

Fig. 1. Convergent auditory mechanisms between mammals and katydids. The three processing stages: (i) sound capture by the TM, (ii) impedance conversion in the middle ear, and (iii) frequency analysis in a fluid-filled dispersive medium. HC, hemolymph channel.

[1]School of Biological Sciences, University of Bristol, Woodland Road, Bristol, BS8 1UG, UK. [2]Imaging Lab, Department of Archaeology and Anthropology, University of Bristol, 43 Woodland Road, Bristol, BS8 1UG, UK.

*To whom correspondence should be addressed. E-mail: fmontealegrez@lincoln.ac.uk (F.M.-Z.); d.robert@bristol.ac.uk (D.R.)

†Present address: School of Life Sciences, Riseholme Campus, University of Lincoln, Lincoln, LN2 2LG, UK.

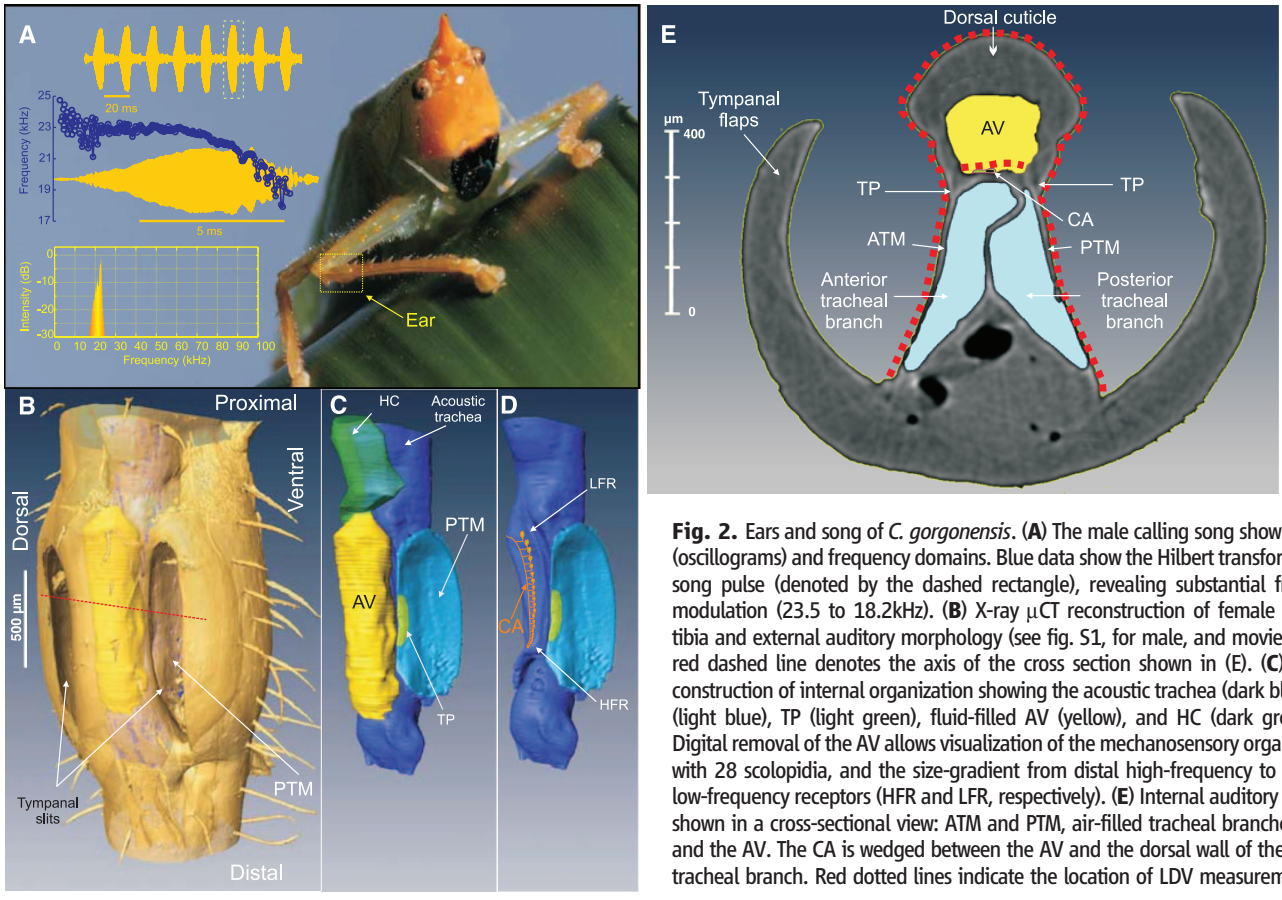

Fig. 2. Ears and song of *C. gorgonensis*. (**A**) The male calling song shown in time (oscillograms) and frequency domains. Blue data show the Hilbert transform of one song pulse (denoted by the dashed rectangle), revealing substantial frequency modulation (23.5 to 18.2kHz). (**B**) X-ray µCT reconstruction of female proximal tibia and external auditory morphology (see fig. S1, for male, and movie S1). The red dashed line denotes the axis of the cross section shown in (E). (**C**) µCT reconstruction of internal organization showing the acoustic trachea (dark blue), PTM (light blue), TP (light green), fluid-filled AV (yellow), and HC (dark green). (**D**) Digital removal of the AV allows visualization of the mechanosensory organ, the CA with 28 scolopidia, and the size-gradient from distal high-frequency to proximal low-frequency receptors (HFR and LFR, respectively). (**E**) Internal auditory anatomy shown in a cross-sectional view: ATM and PTM, air-filled tracheal branches (blue), and the AV. The CA is wedged between the AV and the dorsal wall of the anterior tracheal branch. Red dotted lines indicate the location of LDV measurements.

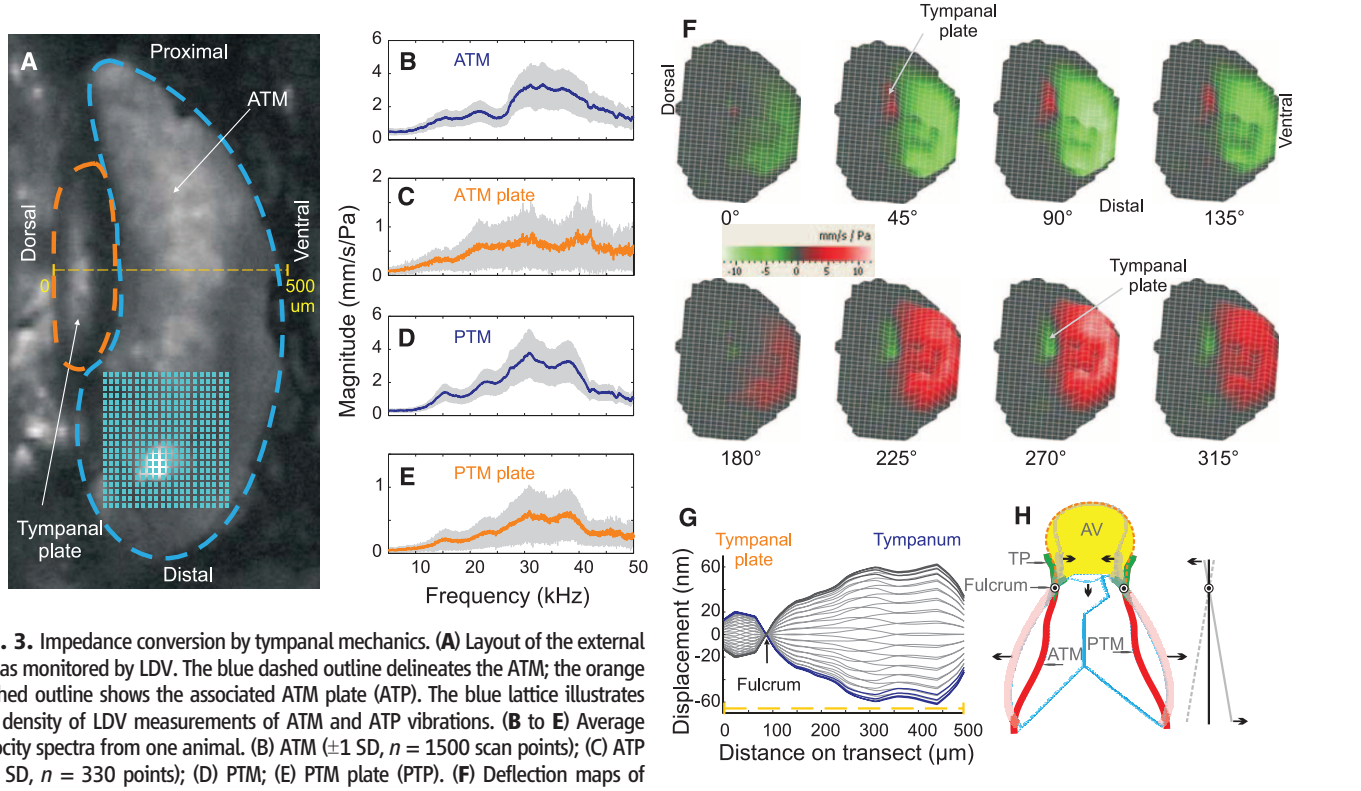

Fig. 3. Impedance conversion by tympanal mechanics. (**A**) Layout of the external ear as monitored by LDV. The blue dashed outline delineates the ATM; the orange dashed outline shows the associated ATM plate (ATP). The blue lattice illustrates the density of LDV measurements of ATM and ATP vibrations. (**B** to **E**) Average velocity spectra from one animal. (B) ATM (±1 SD, n = 1500 scan points); (C) ATP (±1 SD, n = 330 points); (D) PTM; (E) PTM plate (PTP). (**F**) Deflection maps of mechanical responses of ATM and ATP to the 23-kHz tone. Red and green indicate outward and inward deflections, respectively, shown every 45° through one oscillation cycle. (**G**) Deflection envelope of ATM and ATP [across the yellow dashed line in (A)], shown every 10° along the oscillation cycle. ATM and ATP oscillations are exactly out of phase with each other. (**H**) Model of impedance converter, using schematic cross section (Fig. 2E) and lever type 1 analogy.

analytical acoustic stimuli (Fig. 3A). All ear inputs (tympana and spiracles) were exposed to equal sound pressures, using either broadband sounds (5 to 50 kHz) or four-cycle tones at various frequencies, including the 23-kHz calling song (*14*). The auditory frequency range of both TMs exhibits a broad mechanical tuning between 15 and 40 kHz, with a series of maxima in mechanical sensitivity ranging from 20 to 30 kHz (for instance, at 15, 25, 30, and 40 kHz; $n = 21$ animals) (Fig. 3, B and D, and fig. S3).

Both anterior and posterior tympana undergo identical modes of vibration with maximum deflection magnitudes in ventral regions (Fig. 3F), as previously reported in other katydid species (*8*, *15*). From ventral to dorsal side, the TM (Fig. 3A, blue dashed outline) vibrates with steadily decreasing amplitude (Fig. 3F). Extending LDV analysis past the dorsal edge of the TM reveals the vibrations of a cuticular patch, the tympanal plate (TP) (Fig. 3A, orange dashed outline), which makes tight contact with the distal end of the AV. TM and TP vibrations are spectrally similar (Fig. 3, B and E, and fig. S3), indicating that frequency decomposition does not take place at this early stage in the chain of hearing.

Importantly, TM and TP vibrations are 180° out of phase, as illustrated by deflection maps and profiles (Fig. 3G and movie S2). Together, deflection patterns and phase response show that the TM and TP rock around a stationary fulcrum and show rigid connection (Fig. 3G). This rocking behavior is observed for four-cycle tones at any frequency (5 to 50 kHz) and broadband sweeps (fig. S3).

This morphology and mechanical response reveals that the TM-TP system (*14*) acts as an impedance converter analogous to the middle ear ossicles described in terrestrial tetrapods (*16*, *17*). The large deflections of the airborne TM are transformed into smaller deflections of the fluid-bound TP. Thus, this lever system converts a large displacement generated by a small force over a large surface area (sound pressure) (TM) into a small displacement imparting a larger force over a smaller surface area (TP), which is then coupled to AV. From the linear proportions between the TM and TP, the lever ratio is ~10:1 (Fig. 3, G and H). In addition, the ratio between the TM and TP surface areas is 12.94 (±1.12, $n = 21$ animals). The TM-TP system thus operates like a type 1 lever, with at least a 1:10 conversion between effort and load (Fig. 3H). Although TM and TP surface areas are significantly larger in females than in males, male and female TM:TP ratios do not differ (table S1). Amplifying the force imparted by the TMs to the AV and CA, this lever ratio is similar to that reported for the coupling of the tympanal membrane to the cochlea's oval window via the middle ear ossicles in mammals (range: 12.5 to 21.1) (*16*, *18*).

The dorsal cuticle covering the AV between the anterior and posterior tympanal membranes (ATM and PTM, respectively) (Fig. 2E) exhibits a mechanical sensitivity to sound (ratio between response velocity and sound pressure level; millimeters per second per pascal) as high as that observed for the TM and TP (Fig. 4A). Mechanically, this response is representative of AV

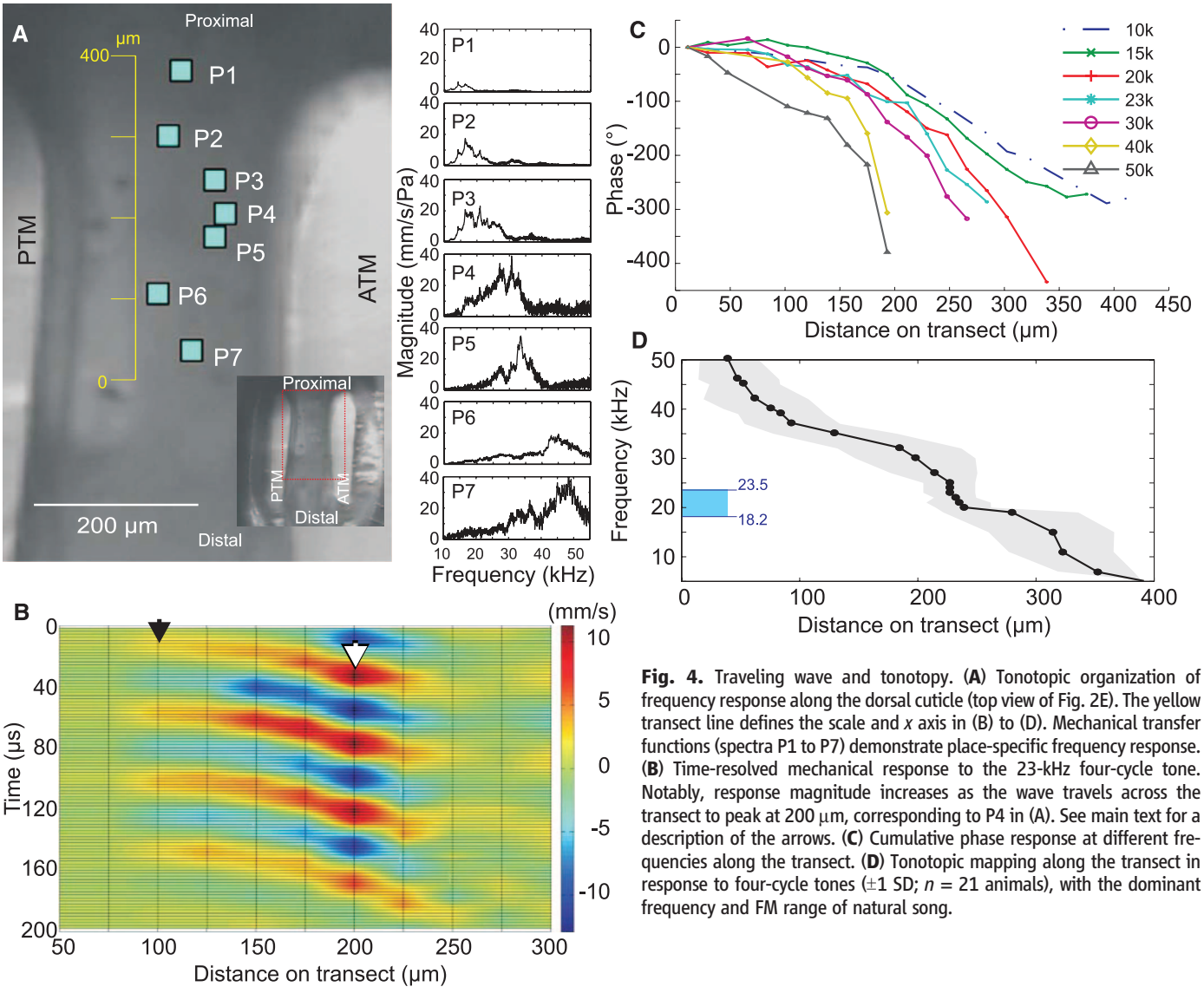

Fig. 4. Traveling wave and tonotopy. (**A**) Tonotopic organization of frequency response along the dorsal cuticle (top view of Fig. 2E). The yellow transect line defines the scale and *x* axis in (B) to (D). Mechanical transfer functions (spectra P1 to P7) demonstrate place-specific frequency response. (**B**) Time-resolved mechanical response to the 23-kHz four-cycle tone. Notably, response magnitude increases as the wave travels across the transect to peak at 200 μm, corresponding to P4 in (A). See main text for a description of the arrows. (**C**) Cumulative phase response at different frequencies along the transect. (**D**) Tonotopic mapping along the transect in response to four-cycle tones (±1 SD; $n = 21$ animals), with the dominant frequency and FM range of natural song.

vibrations, as established by other experiments (figs. S4 to S6) (*14*).

The spatial organization of the frequency response along the dorsal cuticle is in stark contrast with that of the TM and TP. Low frequencies dominate at the proximal end (P1 in Fig. 4A), whereas high frequencies prevail distally (P7 in Fig. 4A; see also fig. S5). This is a hallmark of tonotopy. This organization conforms to the tonotopic sensitivities of CA mechanoreceptors (Fig. 2D) (*11*). Intermediate locations (P2 to P6) exhibit a gradual increase in frequency response.

The definitive characteristics of mammalian cochlear-frequency analyzers are the essential unidirectional traveling waves, discovered by Georg von Békésy (*3*). These features are paralleled at the microscale in katydids by the mechanical deflections observed along the dorsal cuticle (Fig. 4A, yellow line). Traveling waves are initiated distally and travel toward proximal locations of the AV, as recorded through the dorsal cuticle (Fig. 4B and movie S3). A 23-kHz four-cycle tone elicits four oscillations that all reach an identical physical destination, located 200 μm along the transect around location P3-P4 (Fig. 4, A and B). The first cycle elicits a sinusoidal response first located at ~100 μm (Fig. 4B, black arrow), which then moves toward the 200-μm mark (Fig. 4B, white arrow) within 22 μs (half-period at 23 kHz). The oscillation reaches its maximum displacement velocity (red and blue peaks in Fig. 4B) at this position (200 μm), before rapidly decaying over a further 25 μm. The next three cycles generate the same oscillations with increased magnitude at this location. The presence of a wave traveling from distal to proximal locations along the CA corroborates results from another katydid species (*13*). Other frequencies (5 to 50 kHz) also elicit this pattern but reach maximal magnitude at different locations (Fig. 4D). The dispersive nature of AV waves is best illustrated by the presence of phase accumulation, as waves travel across the dorsal cuticle. High-frequency waves (40 to 50 kHz) incur some 260° phase lag within a 200-μm travel length, whereas low-frequency waves (10 kHz), traveling 400 μm, accumulate up to 300° (Fig. 4C). The velocity of wave propagation varies with frequency from 4 ms^{-1} (10 kHz) to 8 ms^{-1} (50 kHz), exhibiting a pattern similar to those reported for mammals and other insects (*13*, *19*).

Deflection shape analysis conducted in the spectral domain (5- to 50-kHz sweeps) confirms the unambiguous presence of traveling waves (fig. S6) (*14*). The data imply that AV provides the anisotropic medium enabling dispersive wave propagation and tonotopic delivery to the auditory receptors. Further experiments establish that both an intact AV and its fluid are required for frequency decomposition as well as for generation of traveling waves (fig. S7). In contrast to observations from the phaneropterine katydid *Mecopoda elongata* (*13*), removal of the dorsal cuticle in *C. gorgonensis* markedly alters AV integrity and eliminates traveling waves and dispersive propagation (*14*).

Altogether, the data show that the impedance conversion, dispersive wave propagation, and tonotopic representation are biophysically analogous to the same qualities of the mammalian cochlea. For *C. gorgonensis*, however, the entire process is embedded in morphology about one to two orders of magnitude smaller than that of mammals (centimeters and millimeters to micrometers).

Frequency representation along the AV covers 10 to 50 kHz (Fig. 4D), a range much larger than that of the natural song (FM: 23.5 to 18.2 kHz) (Fig. 2A) (*6*). Notably, only a short AV segment of ~40 μm represents the song's FM (n = 21 animals) (Fig. 4D). For other frequencies, tonotopic mapping is spatially more disperse (Fig. 4D and fig. S6), suggesting that *C. gorgonensis* can hear other sounds in addition to its own song, such as the ultrasonic sounds of predators (e.g., echolocating bats) (*20*).

As in mammals, impedance matching in katydids arises from the surface area ratio between the TM and TP and from the lever resulting from their coupled action (Fig. 1). Both cases are evolutionarily convergent; the result is the efficient transfer of vibrations to the fluid- or lipid-filled channel (the cochlea or the AV, respectively) where mechanosensory cells reside. Sophisticated hearing is possible at the microscale; katydid ears provide valuable inspiration for the construction of miniaturized smart acoustic sensors, contributing to the expanding panoply of insect-inspired technology.

References and Notes

1. W. Bialek, *Annu. Rev. Biophys. Biophys. Chem.* **16**, 455 (1987).
2. A. J. Hudspeth, *Nature* **341**, 397 (1989).
3. G. von Békésy, *Experiments in Hearing* (McGraw-Hill, New York, 1960).
4. J. Ashmore, *Physiol. Rev.* **88**, 173 (2008).
5. L. Robles, M. A. Ruggero, *Physiol. Rev.* **81**, 1305 (2001).
6. F. Montealegre-Z, M. Postles, *J. Orthoptera Res.* **19**, 347 (2010).
7. J. E. Yack, *Microsc. Res. Tech.* **63**, 315 (2004).
8. M. Bangert *et al*., *Hear. Res.* **115**, 27 (1998).
9. D. B. Lewis, *J. Exp. Biol.* **60**, 839 (1974).
10. K. Kalmring, W. Rossler, R. Ebendt, J. Ahi, R. Lakes, *Zool. Jahrb. Allg. Zool.* **97**, 75 (1993).
11. B. P. Oldfield, *J. Comp. Physiol.* **147**, 461 (1982).
12. R. R. Hoy, D. Robert, *Annu. Rev. Entomol.* **41**, 433 (1996).
13. A. Palghat Udayashankar, M. Kössl, M. Nowotny, *PLoS ONE* **7**, e31008 (2012).
14. Materials and methods are available as supplementary materials on *Science* Online.
15. M. Nowotny, J. Hummel, M. Weber, D. Möckel, M. Kössl, *J. Comp. Physiol. A Neuroethol. Sens. Neural Behav. Physiol.* **196**, 939 (2010).
16. R. Boistel *et al*., *PLoS ONE* **6**, e22080 (2011).
17. J. Mueller, L. A. Tsuji, *PLoS ONE* **2**, e889 (2007).
18. H. A. Thomassen *et al*., *Hear. Res.* **225**, 25 (2007).
19. J. F. C. Windmill, M. C. Göpfert, D. Robert, *J. Exp. Biol.* **208**, 157 (2005).
20. J. J. Belwood, G. K. Morris, *Science* **238**, 64 (1987).

Acknowledgments: This work was sponsored by the Human Frontier Science Program (Cross Disciplinary Fellowship LT00024/2008-C to F.M.-Z.). D.R. is supported by the Royal Society of London. This research was also partially supported by the UK–India Education and Research Initiative (grant no. SA06-169E) and the Biotechnology and Biological Sciences Research Council. We declare no conflict of interest. The Colombian Ministry of Environment granted a permit for fieldwork at Gorgona National Park (decree DTSO-G-31 11/07). All additional information regarding data generation is given in the text and the supplementary materials.

Supplementary Materials

www.sciencemag.org/cgi/content/full/338/6109/968/DC1
Materials and Methods
Supplementary Text
Figs. S1 to S7
Table S1
References (*21*–*32*)
Movies S1 to S3

28 May 2012; accepted 25 September 2012
10.1126/science.1225271

Offspring from Oocytes Derived from in Vitro Primordial Germ Cell–like Cells in Mice

Katsuhiko Hayashi,[1,2,3]* Sugako Ogushi,[1,4] Kazuki Kurimoto,[1,5] So Shimamoto,[1] Hiroshi Ohta,[1,5] Mitinori Saitou[1,2,5,6]*

Reconstitution of female germ cell development in vitro is a key challenge in reproductive biology and medicine. We show here that female (XX) embryonic stem cells and induced pluripotent stem cells in mice are induced into primordial germ cell–like cells (PGCLCs), which, when aggregated with female gonadal somatic cells as reconstituted ovaries, undergo X-reactivation, imprint erasure, and cyst formation, and exhibit meiotic potential. Upon transplantation under mouse ovarian bursa, PGCLCs in the reconstituted ovaries mature into germinal vesicle-stage oocytes, which then contribute to fertile offspring after in vitro maturation and fertilization. Our culture system serves as a robust foundation for the investigation of key properties of female germ cells, including the acquisition of totipotency, and for the reconstitution of whole female germ cell development in vitro.

The germ cell lineage in mammals originates from pluripotent epiblasts as primordial germ cells (PGCs) and undergoes sexually dimorphic development, generating spermatozoa in males and oocytes in females. These cells fertilize to form zygotes with full developmental